

## Electrical transport properties of (BN)-rich hexagonal (BN)C semiconductor alloys

M. R. Uddin,<sup>1</sup> T. C. Doan,<sup>1</sup> J. Li,<sup>1</sup> K. S. Ziemer,<sup>2</sup> J. Y. Lin,<sup>1</sup> and H. X. Jiang<sup>1,a</sup>

<sup>1</sup>Department of Electrical and Computer Engineering, Texas Tech University, Lubbock, TX 79409, USA

<sup>2</sup>Department of Chemical Engineering, Northeastern University, Boston, MA 02115, USA

(Received 30 July 2014; accepted 20 August 2014; published online 29 August 2014)

The layer structured hexagonal boron nitride carbon semiconductor alloys,  $h$ -(BN)C, offer the unique abilities of bandgap engineering (from 0 for graphite to  $\sim 6.4$  eV for  $h$ -BN) and electrical conductivity control (from semi-metal for graphite to insulator for undoped  $h$ -BN) through alloying and have the potential to complement III-nitride wide bandgap semiconductors and carbon based nanostructured materials. Epilayers of (BN)-rich  $h$ -(BN)<sub>1-x</sub>(C<sub>2</sub>)<sub>x</sub> alloys were synthesized by metal-organic chemical vapor deposition (MOCVD) on (0001) sapphire substrates. Hall-effect measurements revealed that homogeneous (BN)-rich  $h$ -(BN)<sub>1-x</sub>(C<sub>2</sub>)<sub>x</sub> alloys are naturally n-type. For alloys with  $x = 0.032$ , an electron mobility of about 20 cm<sup>2</sup>/Vs at 650 °K was measured. X-ray photoelectron spectroscopy (XPS) was used to determine the chemical composition and analyze chemical bonding states. Both composition and chemical bonding analysis confirm the formation of alloys. XPS results indicate that the carbon concentration in the alloys increases almost linearly with the flow rate of the carbon precursor (propane (C<sub>3</sub>H<sub>8</sub>)) employed during the epilayer growth. XPS chemical bonding analysis showed that these MOCVD grown alloys possess more C-N bonds than C-B bonds, which possibly renders the undoped  $h$ -(BN)<sub>1-x</sub>(C<sub>2</sub>)<sub>x</sub> alloys n-type and corroborates the Hall-effect measurement results. © 2014 Author(s). All article content, except where otherwise noted, is licensed under a Creative Commons Attribution 3.0 Unported License. [<http://dx.doi.org/10.1063/1.4894451>]

### I. INTRODUCTION

Both hexagonal boron nitride ( $h$ -BN) and graphite (C) are layer structured materials with similar lattice parameters and crystalline structures. As illustrated in Fig. 1(a), the in-plane  $a$ -lattice constant difference is only about 1.5% between graphite and  $h$ -BN, which provides potential to synthesize layer-structured  $h$ -(BN)<sub>1-x</sub>(C<sub>2</sub>)<sub>x</sub> alloys. The  $h$ -(BN)<sub>1-x</sub>(C<sub>2</sub>)<sub>x</sub> alloy system thus holds the unique advantages of identical crystalline structure (hexagonal) and excellent matches in lattice constants, thermal expansion coefficients, and melting points throughout the entire alloy range. Nevertheless, as schematically shown in Figs. 1(b) and 1(c), this layer-structured alloy system potentially possesses an extremely large energy gap ( $E_g$ ) variation from around 6.4 eV for  $h$ -BN<sup>1-3</sup> to 0 for graphite, following roughly the relation of

$$Eg[h - (BN)_{1-x}(C_2)_x] = (1 - x) Eg(h - BN) + x Eg(C) - b(1 - x)x, \quad (1)$$

where  $E_g(h\text{-BN})$ ,  $E_g(C)$ , and  $b$  are bandgap of  $h$ -BN, bandgap of graphite, and the bowing parameter, respectively.<sup>4</sup> This spectral range exceeds that of the InAlGaN alloy system, which provides tunable band gaps from around 0.64 eV (InN) to 3.4 eV (GaN) to 6.1 eV (AlN).<sup>5,6</sup> From an electrical properties perspective, this alloy system provides a large range of conductivity control from highly

<sup>a</sup>Email: [hx.jiang@ttu.edu](mailto:hx.jiang@ttu.edu)



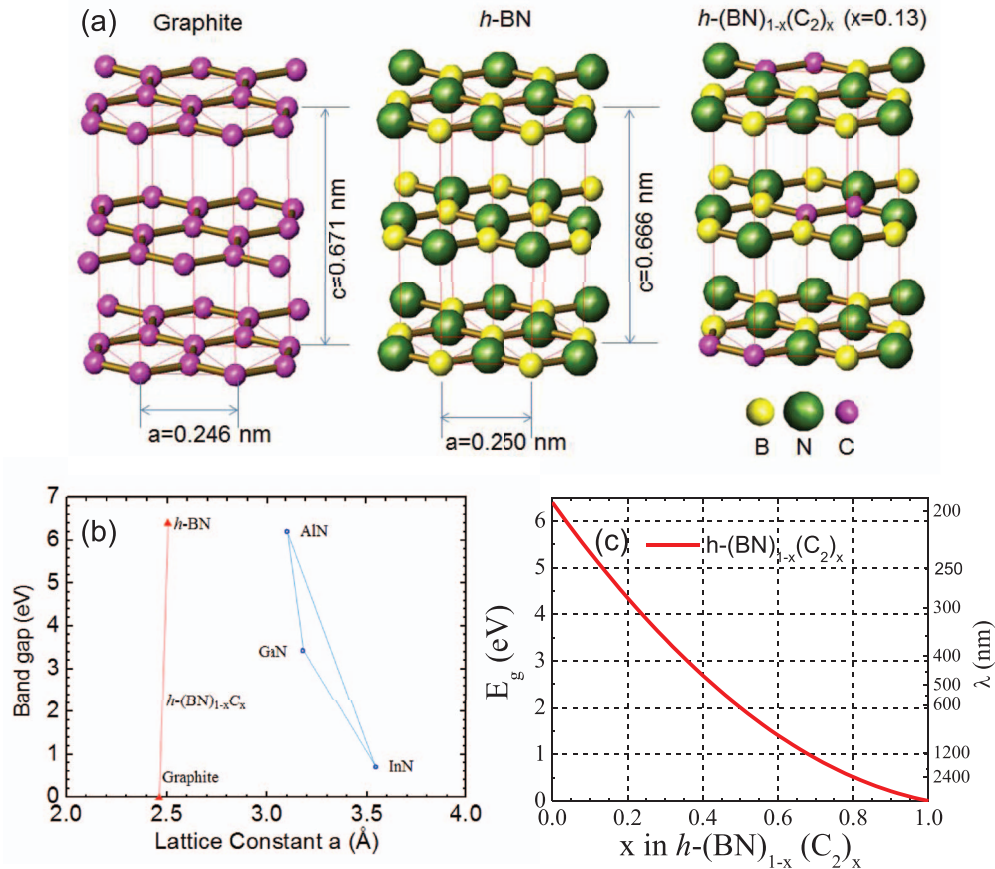


FIG. 1. (a) Schematic illustration of crystal structures of graphite, *h*-BN, and  $h\text{-(BN)}_{1-x}(\text{C}_2)_x$  alloys ( $x \approx 0.13$ ). (b) Comparison of energy bandgap variation with the *a*-lattice constant of  $h\text{-(BN)C}$  alloys with InGaAlN alloys. (c) Bandgap energy and wavelength of  $h\text{-(BN)}_{1-x}(\text{C}_2)_x$  alloys vs carbon concentration (*x*). In the plot, we used the relation  $E_g[h\text{-(BN)}_{1-x}(\text{C}_2)_x] = (1-x)E_g(h\text{-BN}) + xE_g(\text{C}) - b(1-x)x$ , where the bandgap values of  $E_g(h\text{-BN}) = 6.4$  eV and  $E_g(\text{C}) = 0$  eV, and the bowing parameter of  $b = 4.8$  eV were used. In the plot, we also neglected the exciton binding energy, which is about 740 meV in *h*-BN.<sup>1-3</sup>

resistive semiconductors (undoped *h*-BN) to semi-metal (graphite). The  $h\text{-(BN)}_{1-x}(\text{C}_2)_x$  material system would complement III-nitride wide bandgap semiconductors and carbon based nanostructured materials and appears to be highly promising for technologically significant photonic and electronic device applications.<sup>4,7,8</sup> This alloy system is also potentially important low-*k* interconnect material for next generation large scale integrated devices.<sup>9</sup>

Bandgap tuning through compositional variation has been demonstrated recently in  $h\text{-(BN)}_{1-x}(\text{C}_2)_x$  synthesized by metal-organic chemical vapor deposition (MOCVD).<sup>4</sup> Moreover, a variation of approximately 10 orders of magnitude in the electrical conductivity has been attained by changing the carbon concentration (*x*) from 0 to 0.21.<sup>4</sup> A previous study noted that the unintentionally doped  $h\text{-(BN)}_{1-x}(\text{C}_2)_x$  in the middle composition range ( $h\text{-(BN)}_{0.5}\text{C}_{0.5}$ ) synthesized by chemical vapor deposition are p-type.<sup>10</sup> However, the origins of the carrier types and the roles of chemical bonding in conductivity control have not been examined in this alloy system.

In this work, we carried out X-ray photoelectron spectroscopy (XPS) and carrier mobility studies on (BN)-rich  $h\text{-(BN)}_{1-x}(\text{C}_2)_x$  alloys grown by MOCVD. While MOCVD is an established technique for producing high quality crystalline materials due to its ability to precisely control the growth processes and has been widely adopted by the commercial sector for producing wide bandgap semiconductors in large wafer scales, the technique is being adopted for the growth of  $h\text{-(BN)C}$  alloys only very recently.<sup>4</sup> On the other hand, XPS is a quantitative spectroscopic technique with capabilities to provide information regarding the sample uniformity, elemental composition,

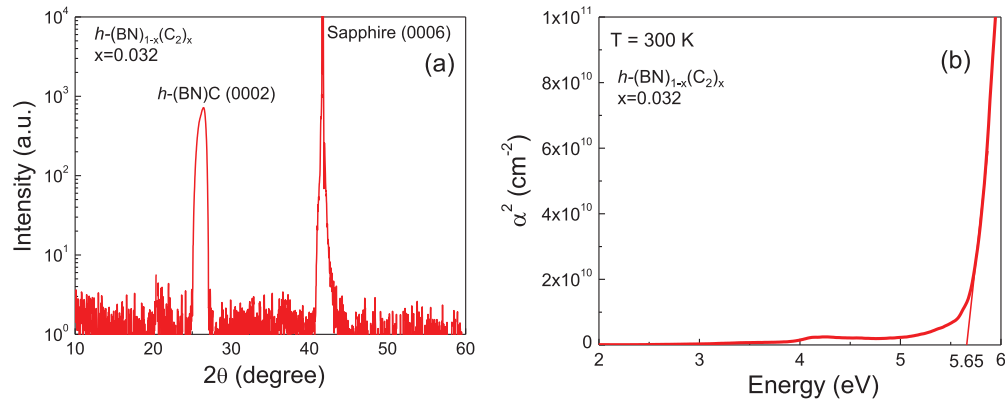


FIG. 2. (a) XRD  $\theta$ - $2\theta$  scan of a  $h$ -(BN) $_{1-x}$ (C $_2$ ) $_x$  alloy with  $x = 0.032$  and a thickness of 60 nm grown on  $c$ -plane sapphire; (b) Tauc plot of the optical absorption coefficient of the same sample.

and chemical bonding states of the constituents within a material,<sup>11</sup> which can aid greatly the development of  $h$ -(BN)C alloys with improved quality.<sup>12–14</sup> Hall-effect measurements showed that (BN)-rich  $h$ -(BN) $_{1-x}$ (C $_2$ ) $_x$  alloys exhibit  $n$ -type conductivity. XPS results revealed that these alloys possess more C-N bonds than C-B bonds, making undoped (BN)-rich  $h$ -(BN)C alloys naturally  $n$ -type.

## II. EXPERIMENTS

Thin films of  $h$ -(BN) $_{1-x}$ (C $_2$ ) $_x$  alloys of about 60 nm in thickness were deposited on  $c$ -plane single crystal sapphire at 1300 °C using triethylboron (TEB), ammonia (NH $_3$ ), and propane (C $_3$ H $_8$ ) as B, N, and C precursors, respectively. Samples were grown using hydrogen as a carrier gas. Six samples were grown using C $_3$ H $_8$  flow rates of 0.5, 1, 2, 3, 4, and 5 standard cubic centimeters per minute (sccm). Both TEB and NH $_3$  flow rates were kept constant at 0.06 sccm and 3 standard liter per minute (SLM), respectively (corresponding nitrogen-rich conditions). Carbon to boron (C:B) ratio is varied from  $\sim 8$  to 80 for a C $_3$ H $_8$  flow rate from 0.5 sccm to 5 sccm. Figure 2(a) shows a representative X-ray diffraction (XRD)  $\theta$ - $2\theta$  scan of a  $h$ -(BN) $_{1-x}$ (C $_2$ ) $_x$  sample with  $x = 0.032$  revealing a lattice constant of  $c = 6.70$  Å, which closely matches with a value of  $c = 6.67$  Å for hexagonal BN ( $h$ -BN) epilayers grown at the same temperature<sup>15,16</sup> and also with that of graphite (Fig. 1(a)). No other diffraction peaks were observed indicating that (BN) $_{1-x}$ (C $_2$ ) $_x$  samples with  $x \leq 0.032$  are of hexagonal phase. Figure 2(b) shows the optical absorption spectrum for a  $h$ -(BN) $_{1-x}$ (C $_2$ ) $_x$  sample with  $x = 0.032$ , revealing an apparent optical bandgap of around  $\sim 5.65$  eV. However, our previous experimental results revealed evidences that the critical carbon concentration ( $x_c$ ) for the formation of homogenous  $h$ -(BN) $_{1-x}$ (C $_2$ ) $_x$  alloys, or the carbon solubility in  $h$ -BN is about 3.2% at the growth temperature of 1300 °C before carbon clusters form.<sup>4</sup>

The XPS experiments were performed with a PHI 5000 VersaProbe Electron Spectroscopy for Chemical Analysis (ESCA) spectrometer using a focused monochromatic Al K $\alpha$  ( $h\nu = 1486.6$  eV) X-ray beam with a diameter of 100  $\mu$ m. In order to determine the atomic concentrations in the alloys accurately and to eliminate possible surface contamination by impurities from atmosphere before XPS measurements, we adopted the process of surface cleaning with low energy (500 V) Ar $^+$  ion sputtering. Initial survey scans were performed using pass energy of 187.85 eV with an energy step of 0.8 eV, while high resolution tight scans were performed using pass energy of 23.50 eV at an energy step of 0.1 eV. The binding energy scales of the samples were referenced to the C-C bonding peak at 284.8 eV in order to eliminate the effect of any surface charging. For all samples, we analyzed the uniform area to avoid any effect of the sample non-uniformity. Data were analyzed consistently using Multipak software.

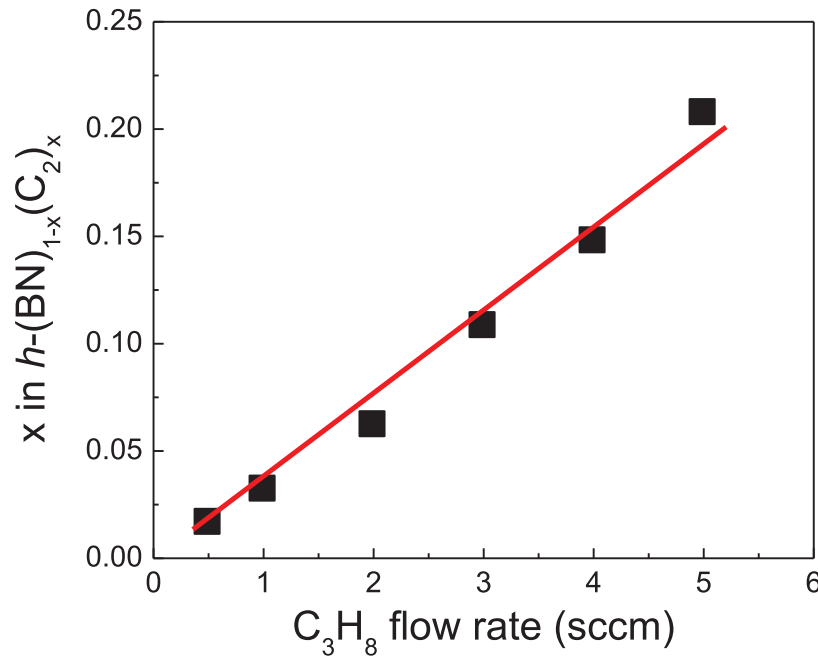


FIG. 3. The carbon atomic composition ( $x$ ) in  $h\text{-(BN)}_{1-x}(\text{C}_2)_x$  alloys as a function of the  $\text{C}_3\text{H}_8$  flow rate employed during MOCVD growth. The values of  $x$  were determined from high resolution XPS tight scans after removing surface contaminants using  $\text{Ar}^+$  ion sputtering.

### III. RESULTS AND DISCUSSION

Figure 3 shows the carbon atomic composition ( $x$ ) in  $h\text{-(BN)}_{1-x}(\text{C}_2)_x$  as a function of the  $\text{C}_3\text{H}_8$  flow rate employed during MOCVD growth for the six samples grown using  $\text{C}_3\text{H}_8$  flow rates of 0.5, 1, 2, 3, 4, and 5 sccm, where  $x$  values were determined from high resolution XPS tight scans after removing surface contaminants using  $\text{Ar}^+$  ion sputtering. The measured carbon concentrations were 1.7%, 3.2%, 6.2%, 10.8%, 14.8%, and 20.8% for the six samples grown using  $\text{C}_3\text{H}_8$  flow rates of 0.5, 1, 2, 3, 4, and 5 sccm, respectively. XPS measurements thus establish that the C concentration increases almost linearly with an increase of the  $\text{C}_3\text{H}_8$  flow rate employed during growth, providing a linear calibration for future growth optimization.

A unique feature of the  $h\text{-(BN)}_{1-x}(\text{C}_2)_x$  alloy system is that it offers the conductivity variation from highly insulating semiconductor (undoped  $h\text{-BN}$ ) to semi-metal (graphite). We have shown that the room temperature electrical resistivity decreases approximately by 10 orders of magnitude from  $\sim 10^{11} \Omega \cdot \text{cm}$  to  $\sim 10 \Omega \cdot \text{cm}$  when  $x$  increases from 0 to 0.21.<sup>4</sup> However, the electrical conductivity type has not been determined. In order to determine the carrier type, we have attempted Van der Pauw-Hall effect measurements<sup>17</sup> on these samples. Due to the large band gaps and highly resistive nature, the Hall-effect measurements could not be made on undoped  $h\text{-BN}$  and  $h\text{-(BN)}_{1-x}(\text{C}_2)_x$  alloys with  $x < 0.032$  at any temperatures. For the sample with  $x = 0.032$ , which has been verified to form a homogeneous alloy,<sup>4</sup> we were able to perform the van der Pauw-Hall measurements at high temperatures,  $T > 600^\circ\text{K}$ . Efforts were made to minimize the impact of sample non-uniformity or inhomogeneity on the measured carrier type. This was achieved via the use of square shaped sample geometry with triangular ohmic contacts fabricated on the four corners of the sample.<sup>18–20</sup> The microscope image of a fabricated  $h\text{-(BN)}_{1-x}(\text{C}_2)_x$  alloy ( $x = 0.032$ ) sample with ohmic contact (Ni/Au bilayers) geometry employed is shown in Fig. 4(a). The ratio of the contact size ( $c$ ) to the sample length scale ( $L$ ) is about 1/7.5, a configuration which is expected to provide a high confidence in the measured carrier type.<sup>18</sup> Ohmic contact processing procedures were adopted from those developed from pure  $h\text{-BN}$  epilayers<sup>20</sup> and the ohmic behavior is evident based on the linear I-V characteristic shown in Fig. 4(b).

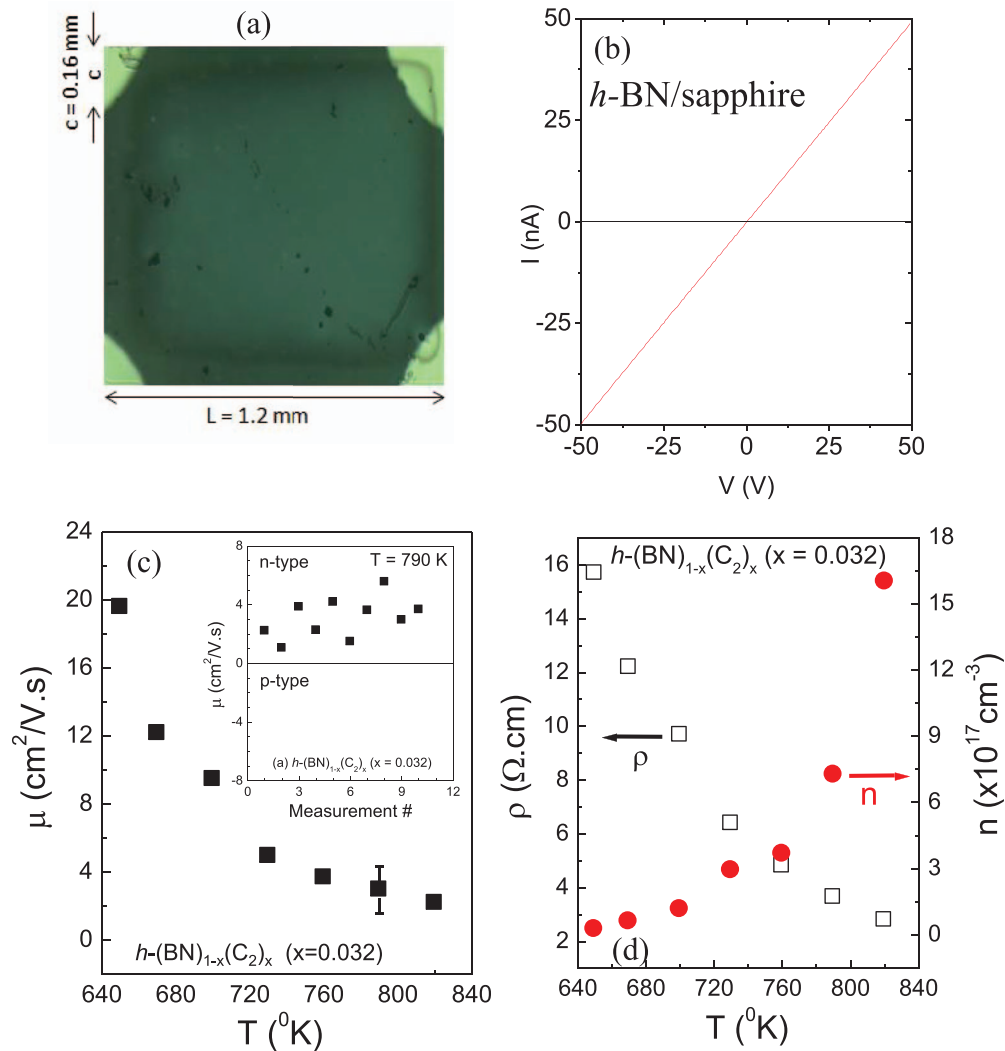


FIG. 4. Electrical transport properties of  $h$ -(BN) $_{1-x}$ (C $_2$ ) $_x$  alloy films with  $x = 0.032$ : (a) The microscope image of a  $h$ -(BN) $_{1-x}$ (C $_2$ ) $_x$  alloy ( $x = 0.032$ ) sample with ohmic contact (Ni/Au bilayers) geometry employed for van der Pauw–Hall measurements. (b) Demonstration of the ohmic behavior of the metal contacts used. (c) Electron mobility as a function of temperature and the inset shows the electron mobility data measured at  $790^\circ\text{K}$ . In our experimental setup,  $+\mu$  means electron conduction and  $-\mu$  means hole conduction. (d) Electrical resistivity and electron concentration as functions of temperature.

The variations of the electron mobility, the electron concentration and resistivity of  $h$ -(BN) $_{1-x}$ (C $_2$ ) $_x$  alloy ( $x = 0.032$ ) with temperature are shown in Fig. 4(c) and 4(d), respectively. As the temperature was increased from  $650$  to  $820^\circ\text{K}$ , the measured resistivity and electron mobility decreased, respectively, from  $15.7$  to  $2.6 \Omega\cdot\text{cm}$  and  $19.6$  to  $2.2 \text{ cm}^2/\text{Vs}$ , while the electron concentration increased from  $2.6 \times 10^{16}$  to  $1.5 \times 10^{18} \text{ cm}^{-3}$ . The results demonstrate the characteristics of a wide bandgap semiconductor.

Due to the formation of random alloy as well as an adequate resistivity of the  $h$ -(BN) $_{1-x}$ (C $_2$ ) $_x$  sample with  $x = 0.032$ , we were able to measure the mobility and determine the electrical conductivity type at high temperatures. As illustrated in the inset of Fig. 4(c), Hall-effect measurements carried out at  $T = 790^\circ\text{K}$  for the sample with  $x = 0.032$  for multiple times yielded an average mobility of  $\mu \sim 3 \text{ cm}^2/\text{V}\cdot\text{s}$ . The mobility data consist of a sizeable variation, however, unambiguously confirmed that (BN)-rich  $h$ -(BN) $_{1-x}$ (C $_2$ ) $_x$  alloys exhibit n-type conductivity. It is quite remarkable that these alloys exhibit a mobility value as high as  $15.7 \text{ cm}^2/\text{Vs}$  at  $650^\circ\text{K}$  in such an early phase of the

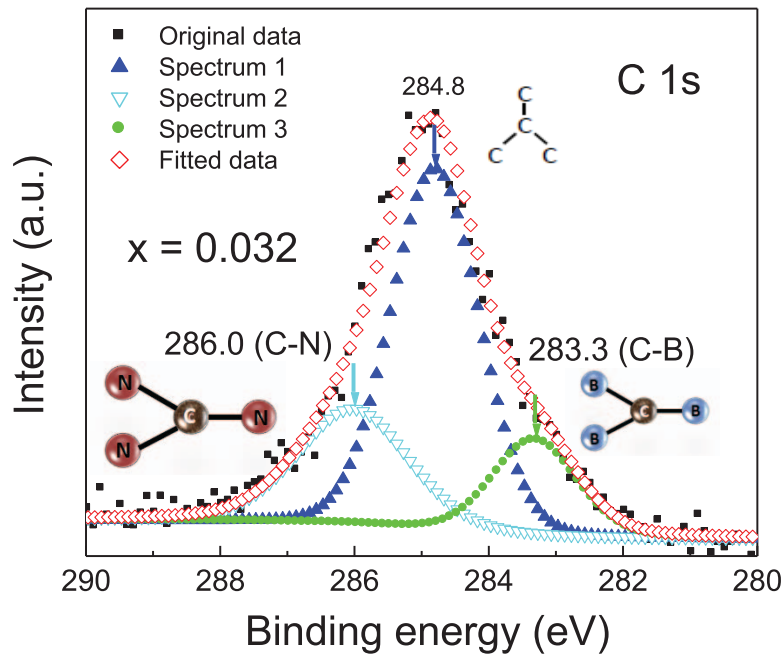


FIG. 5. XPS spectra of C 1s core level for the  $h\text{-(BN)}_{1-x}\text{(C}_2)_x$  alloy with  $x = 0.032$ . The inset are schematic illustrations of C-N and C-B bonds in (BN)-rich  $h\text{-(BN)}_{1-x}\text{(C}_2)_x$  alloys.

materials development. In comparison, the highest electron mobility reported for Si doped n-type AlN, which has a comparable bandgap of about 6 eV, is  $\sim 100 \text{ cm}^2/\text{Vs}$  at 600 K.<sup>21</sup>

Figure 5 shows XPS spectra of the C 1s core level for  $h\text{-(BN)}_{1-x}\text{(C}_2)_x$  alloy with  $x = 0.032$ . The spectrum was fitted by subtracting a Shirley background<sup>22</sup> with a Gauss-Lorentz function. The peak was shifted with respect to the fortuitous carbon before any analysis is made. Spectrum 1 shows the main peak at 284.8 eV, which is similar to that of  $\text{sp}^2$  bonded C-C (graphite). However, the full width at half maximum (FWHM) of this peak is 1.55 eV, which is significantly higher than our graphite (0.70 eV) sample grown under the same conditions. This confirms that there is a significant contribution from C-B and C-N bonds in this alloy system. Indeed there are two additional peaks in both sides of the main peak, indicated as spectrum 2 and spectrum 3, respectively. The lower energy peak at 283.3 eV (spectrum 2) is due to C bonding with B (C-B).<sup>23–25</sup> The higher energy peak at 286.0 eV (spectrum 3) is due to C bonding with N (C-N).<sup>26</sup> The chemical shifts, peak broadening, and bonding analysis described above indicate that boron, carbon, and nitrogen atoms bond with one another, and mix atomically.

We believe that the presence of specific bonding states have consequences on the conductivity type of unintentionally doped (BN)-rich  $h\text{-(BN)}_{1-x}\text{(C}_2)_x$  alloys. For instances, the observation of C-N bonds in (BN)-rich  $h\text{-(BN)C}$  alloys represents the scenario of a fraction of C atoms replacing B ( $\text{C}_B$ ), in which C atoms act as n-type dopants. Stated in another way, the detection of C-B bonds in (BN)-rich  $h\text{-(BN)}_{1-x}\text{(C}_2)_x$  alloys means that a fraction of C atoms are replacing N ( $\text{C}_N$ ) and C act as p-type dopants. Detail studies of the B 1s and N 1s peaks have been carried out and their bonding states are essential in the understanding of the formation of  $h\text{-(BN)C}$  alloy.<sup>4</sup> However, further analysis of B 1s and N 1s spectra does not provide useful information regarding the electrical conductivity type.

For the sample with  $x = 0.032$ , C-N peak (286.0 eV) intensity is stronger than the C-B peak (283.3 eV). The corresponding integrated intensity (peak  $\times$  area) of the C-N peak is about 1.6 times larger than the C-B peak. XPS results shown in Fig. 5 thus imply that the films contain more C-N bonds than C-B bonds, which means that more C atoms are replacing B than those replacing N, which may account for the observed n-type conductivity in (BN)-rich  $h\text{-(BN)}_{1-x}\text{(C}_2)_x$  alloys. This interpretation is also consistent with the understanding from the point of view of bond energies

among different bonds in  $h\text{-(BN)}_{1-x}\text{(C}_2\text{)}_x$  alloy: B-N (4.00 eV) > C-C (3.71 eV) > C-N (2.83 eV) > C-B (2.59 eV) > B-B (2.32 eV) > N-N (2.11 eV). The formation of C-N bonds is more favorable than the formation of C-B bonds due to the larger bond energy of C-N bond.<sup>27</sup> Although most C atoms incorporate into  $h\text{-(BN)}_{1-x}\text{(C}_2\text{)}_x$  alloys as pairs due to the relatively large C-C bond energy, from the statistics point of view, there is always a certain fraction of C remains in the isolated state, which can either replace B to provide n-type dopants or replace N to provide p-type dopants. From the formation energy point of view, the formation of C-N bond is also more favorable over that of C-B bond.<sup>27</sup> The presence of more C-N bonds than C-B bonds makes undoped (BN)-rich  $h\text{-(BN)}_{1-x}\text{(C}_2\text{)}_x$  semiconductor alloys n-type. Thus the XPS results corroborate the mobility data shown in Fig. 4. A very small fraction of excess C-N bonds ( $\sim 10^{19}/10^{22}$ ) can have a significant effect on the electrical conductivity type but not on the variation in composition. Therefore, it is difficult to detect and quantify the variation in composition due to the presence of excess C-N bonds.

#### IV. CONCLUSIONS

In summary, thin films of (BN)-rich  $h\text{-(BN)}_{1-x}\text{(C}_2\text{)}_x$  semiconductor alloys were synthesized by MOCVD. Hall-effect measurements revealed that these alloys are naturally n-type exhibiting an electron mobility of about 20 cm<sup>2</sup>/Vs at 650 °K. XPS results indicated that the carbon concentration in the alloys increases almost linearly with the flow rate of the carbon precursor employed during the MOCVD growth, providing a useful calibration for targeted alloy compositions. XPS chemical bonding analysis revealed that these MOCVD grown alloy films contain more C-N bonds than C-B bonds, making (BN)-rich  $h\text{-(BN)}_{1-x}\text{(C}_2\text{)}_x$  alloys naturally n-type. Currently, our understanding of  $h\text{-(BN)}_{1-x}\text{(C}_2\text{)}_x$  alloy is still in a very early stage. XPS studies coupled with optical and transport measurements are useful for providing insights into further developing strategies to obtain materials with improved quality and conductivity control as well as the fundamental understanding on the alloy dependence of the band structures, optical and optoelectronic properties of this emerging layer-structured material system.

#### ACKNOWLEDGMENTS

This work is supported by NSF (DMR-1206652). Jiang and Lin are grateful to the AT&T Foundation for the support of Ed Whitacre and Linda Whitacre endowed chairs.

- <sup>1</sup> B. Arnaud, S. Lebègue, P. Rabiller, and M. Alouani, *Phys. Rev. Lett.* **96**, 026402 (2006).
- <sup>2</sup> B. Huang, X. K. Cao, H. X. Jiang, J. Y. Lin, and S. H. Wei, *Physical Review B* **86**, 155202 (2012).
- <sup>3</sup> X. K. Cao, B. Clubine, J. H. Edgar, J. Y. Lin, and H. X. Jiang, *Appl. Phys. Lett.* **103**, 191106 (2013).
- <sup>4</sup> M. R. Uddin, S. Majety, J. Li, J. Y. Lin, and H. X. Jiang, *J. Appl. Phys.* **115**, 093509 (2014).
- <sup>5</sup> S. Nakamura, G. Fasol, and S. J. Pearton, *The Blue Laser Diode: The Complete Story*, (Springer, New York, 2000).
- <sup>6</sup> J. Wu, *J. Appl. Phys.*, **106**, 011101 (2009).
- <sup>7</sup> M. O. Watanabe, S. Itoh, T. Sasaki, and K. Mizushima, *Phys. Rev. Lett.* **77**, 187 (1996).
- <sup>8</sup> M. O. Watanabe, K. Mizushima, S. Itoh, and M. Mashita, "Semiconductor device using semiconductor BCN compounds," U.S. patent 5,895, 938.
- <sup>9</sup> S. Umeda, T. Yuki, T. Sugiyama, and T. Sugino, *Diamond Relat. Mater.* **13**, 1135 (2004).
- <sup>10</sup> M. O. Watanabe, S. Itoh, K. Mizushima, and T. Sasaki, *J. Appl. Phys.* **78**, 2880 (1995).
- <sup>11</sup> D. Briggs and M. P. Seah, *Practical surface analysis by Auger and X-ray photoelectron spectroscopy* (Wiley, New York, 1990).
- <sup>12</sup> J. R. Martins and H. Chacham, *ACS Nano* **5**, 385 (2011).
- <sup>13</sup> M. O. Watanabe, S. Itoh, K. Mizushima, and T. Sasaki, *Appl. Phys. Lett.* **68**, 2962 (1996).
- <sup>14</sup> V. Linss, S. E. Rodil, P. Reinke, M. G. Garnier, P. Oelhafen, U. Kreissig, and F. Richter, *Thin Solid Films* **467**, 76 (2004).
- <sup>15</sup> R. Dahal, J. Li, S. Majety, B. N. Pantha, X. K. Cao, J. Y. Lin, and H. X. Jiang, *Appl. Phys. Lett.* **98**, 211110 (2011).
- <sup>16</sup> J. Li, S. Majety, R. Dahal, W. P. Zhao, J. Y. Lin, and H. X. Jiang, *Appl. Phys. Lett.* **101**, 171112 (2012).
- <sup>17</sup> L. J. Van der Pauw, *Philips Research Reports*, **13**, 1 (1958).
- <sup>18</sup> O. Bierwagen, T. Ive, C. G. Van de Walle, and J. S. Speck, *Appl. Phys. Lett.* **93**, 242108 (2008).
- <sup>19</sup> A. Kumar, J. Pernot, F. Omnès, P. Muret, A. Traoré, L. Magaud, A. Deneuille, N. Habka, J. Barjon, F. Jomard, M. A. Pinault, J. Chevallier, C. Mer-Calfati, J. C. Arnault, and P. Bergonzo, *J. Appl. Phys.* **110**, 033718 (2011).
- <sup>20</sup> S. Majety, T. C. Doan, J. Li, J. Y. Lin, and H. X. Jiang, *AIP Advances* **3**, 122116 (2013).
- <sup>21</sup> Y. Taniyasu, M. Kasu, and T. Makimoto, *Nature*, **441**, 325 (2006).
- <sup>22</sup> D. A. Shirley, *Phys. Rev. B* **5**, 4709 (1972).
- <sup>23</sup> H. Kunzli, P. Gantenbein, R. Steiner, and P. Oelhafen, *Anal. Chem.* **346**, 41 (1993).

- <sup>24</sup>H. A. Castillo, P. J. Arango, J. M. Velez, E. Restrepo-Parra, G. Soto, and W. D. la Cruz, [Surf. Coat. Technol.](#) **204**, 4051 (2010).
- <sup>25</sup>J. Yue, W. Cheng, X. Zhang, D. He, and G. Chen, [Thin Solid Films](#) **375**, 247 (2000).
- <sup>26</sup>E. G. Wang, [Prog. Mater. Sci.](#) **41**, 241 (1997).
- <sup>27</sup>M. S. C. Mazzoni, R. W. Nunes, S. Azedevo, and H. Chacham, [Phys. Rev. B](#) **73**, 073108 (2006).